3D Snap Rounding

Olivier Devillers, Sylvain Lazard, William Lenhart

3D Snap Rounding

Olivier Devillers
Université de Lorraine, CNRS, Inria, LORIA
F-54000 Nancy, France

Sylvain Lazard
Université de Lorraine, CNRS, Inria, LORIA
F-54000 Nancy, France
sylvain.lazard@inria.fr

William J. Lenhart
Williams College
Williamstown, Massachusetts, USA

Abstract

Let $\mathcal{P}$ be a set of n polygons in $\mathbb{R}^3$, each of constant complexity and with pairwise disjoint interiors. We propose a rounding algorithm that maps $\mathcal{P}$ to a simplicial complex $\mathcal{Q}$ whose vertices have integer coordinates. Every face of $\mathcal{P}$ is mapped to a set of faces (or edges or vertices) of $\mathcal{Q}$ and the mapping from $\mathcal{P}$ to $\mathcal{Q}$ can be done through a continuous motion of the faces such that (i) the L_∞ Hausdorff distance between a face and its image during the motion is at most $3/2$ and (ii) if two points become equal during the motion, they remain equal through the rest of the motion. In the worst case, the size of $\mathcal{Q}$ is $O(n^{15})$ and the time complexity of the algorithm is $O(n^{19})$ but, under reasonable hypotheses, these complexities decrease to $O(n^5)$ and $O(n^6\sqrt{n})$.

2012 ACM Subject Classification Theory of computation → Computational geometry

Keywords and phrases Geometric algorithms, Robustness, Fixed-precision computations

Digital Object Identifier 10.4230/LIPIcs.SoCG.2018.30

Related Version A full version of this paper is available at `https://hal.inria.fr/hal-01698928`

1 Introduction

Rounding 3D polygonal structures is a fundamental problem in computational geometry. Indeed, many implementations dealing with 3D polygonal objects, in academia and industry, require as input pairwise-disjoint polygons whose vertices have coordinates given with fixed-precision representations (usually with 32 or 64 bits). On the other hand, many algorithms and implementations dealing with 3D polygonal objects in computational geometry output polygons whose vertices have coordinates that have arbitrary-precision representations. For instance, when computing boolean operations on polyhedra, some new vertices are defined as the intersection of three faces and their exact coordinates are rational numbers whose numerators and denominators are defined with roughly three times the number of bits used for representing each input coordinate. When applying a rotation to a polyhedron, the new vertices have coordinates that involve trigonometric functions. When sampling algebraic surfaces, the vertices are obtained as solutions of algebraic systems and they may require arbitrary-precision representations since the distance between two solutions may be arbitrarily small (depending on the degree of the surface).

This discrepancy between the precision of the input and output of many geometric algorithms is an issue, especially in industry, because it often prevents the output of one algorithm from being directly used as the input to a subsequent algorithm.

34th International Symposium on Computational Geometry (SoCG 2018).
Editors: Bettina Speckmann and Csaba D. Tóth; Article No. 30; pp. 30:1–30:14
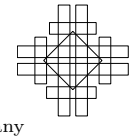

Leibniz International Proceedings in Informatics
Schloss Dagstuhl – Leibniz-Zentrum für Informatik, Dagstuhl Publishing, Germany

In this context, there exists no solution for rounding the coordinates of 3D polygons with the constraint that their rounded images do not properly intersect and that every input polygon and its rounded image remain close to each other (in Hausdorff distance). In practice, coordinates are often rounded without guarding against changes in topology and there is no guarantee that the rounded faces do not properly intersect one another.

The same problem in 2D for segments, referred to as snap rounding, has been widely studied and admits practical and efficient solutions [1, 5–11, 14]. Given a set of possibly intersecting segments in 2D, the problem is to subdivide their arrangement and round the vertices so that no two disjoint segments map to segments that properly intersect. For clarity, all schemes consider that vertices are rounded on the integer grid. It is well known that rounding the endpoints of the edges of the arrangement to their closest integer point is not a good solution because it may map disjoint segments to properly intersecting segments.. Snap rounding schemes propose to further split the edges when they share a pixel (a unit square centered on the integer grid). In such schemes, disjoint edges may collapse but this is inevitable if the rounding precision is fixed and if we bound the Hausdorff distance between the edges and their rounded images. Furthermore, it is NP-hard to determine whether it is possible to round simple polygons with fixed precision and bounded Hausdorff distance, and without changing the topological structure [12].

In dimension three, results are extremely scarse, despite the significance of the problem. Goodrich et al. [5] proposed a scheme for rounding segments in 3D, and Milenkovic [13] sketched a scheme for polyhedral subdivisions but, as pointed out by Fortune [4], both schemes have the property that rounded edges can cross. Fortune [3] suggested a high-level rounding scheme for polyhedra but in a specific setting that does not generalize to polyhedral subdivisions [4]. Finally, Fortune [4] proposed a rounding algorithm that maps a set $\mathcal{P}$ of n disjoint triangles in $\mathbb{R}^3$ to a set $\mathcal{Q}$ of triangles with $O(n^4)$ vertices on a discrete grid such that (i) every triangle of $\mathcal{P}$ is mapped to a set of triangles in $\mathcal{Q}$ at L_∞ Hausdorff distance at most $\frac{3}{2}$ from the original face and (ii) the mapping preserves or collapses the vertical ordering of the faces. Unfortunately, this rounding scheme is very intricate and, moreover, it uses a grid precision that depends on the number n of triangles: the vertices coordinates are rounded to integer multiples of about $\frac{1}{n}$.

The difficulty of snap rounding faces in 3D is described by Fortune [4]: First, it is reasonable to round every vertex to the center of the voxel containing it (a voxel is a unit cube centered on the integer grid). But, by doing so, a vertex may traverse a face and to avoid that, it might be necessary to add beforehand a vertex on the face, which requires triangulating it. Newly formed edges may cross older edges when snapping; to avoid this, new vertices are added to these edges, in turn requiring further triangulating of faces. It is not known whether such schemes terminate.

To better understand the difficulty of the problem, consider the following simple but flawed algorithm. First project all the input faces onto the horizontal plane, subdivide the projected edges as in 2D snap rounding, triangulate the resulting arrangement, lift this triangulation vertically on all faces, and then round all vertices to the centers of their voxels. For an input of size n, this yields an output of size $\Theta(n^4)$ in the worst case and an L_∞ Hausdorff distance of at most $\frac{1}{2}$ between the input faces and their rounded images. Unfortunately, this algorithm does not work in the sense that edges may cross: indeed, consider two almost vertical close triangles whose projections on the horizontal plane are disjoint triangles that are rounded in 2D to the same segment; such triangles in 3D may be rounded into properly overlapping triangles. Fortune [4] solved this problem by using a finer grid to round the vertices and to avoid vertical rounding of the faces.

Contributions. We present in this paper the first algorithm for rounding a set of interior-disjoint polygons into a simplicial complex whose vertices have integer coordinates and such that the geometry does not change too much: namely, (i) the Hausdorff distance between every input face and its rounded image is bounded by a constant ($\frac{3}{2}$ for the L_∞ metric) and (ii) the relative positions of the faces are preserved in the sense that there is a continuous motion that deforms all input faces into their rounded images such that if two points collapse at some time, they remain identical up to the end of the motion (see Thm. 1). This ensures, in particular, that if a line stabs two input faces far enough from their boundaries, the line will stab their rounded images in the same order or in the same point.

The worst-case complexity of our algorithm is polynomial but unsatisfying as our upper bound on the output simplicial complex is $O(n^{15})$ for an input of size n (see Prop. 7). However, this upper bound decreases to $O(n^5)$ under the assumption that, roughly speaking, the input is a nice discretization of a constant number of surfaces that satisfy some reasonable hypothesis on their curvature (see Prop. 13 for details). The corresponding time complexity reduces from $O(n^{19})$ to $O(n^6\sqrt{n})$. It is also very likely that these bounds are not tight and, in practice on realistic non-pathological data, we anticipate time and space complexities of $O(n\sqrt{n})$ (see Remark 14).

Notation. The coordinates in the Euclidean space $\mathbb{R}^3$ are referred to as x, y, and z and $\vec{\imath}, \vec{\jmath}, \vec{k}$ is the canonical basis. We use several planes parallel to the axes to project or intersect some faces: the xy-plane is called the *floor*, the xz-plane is called the *back wall* and a plane parallel to the yz-plane is called a *side wall*. Projections on the floor and on the back wall are always considered orthogonal to the plane of projection.

Two polygons, edges, or vertices are said to *properly intersect* if their intersection is non-empty and not a common face of both. Two polygons (resp. segments) intersect transversally if their relative interiors intersect and if they are not coplanar (resp. collinear).

General position assumption. For the sake of simplicity, we assume, without loss of generality, some general position on our input set of polygons $\mathcal{P}$. Precisely, we assume:

(α) No faces are parallel to the axes of coordinates and no vertices project along the y-axis on an edge (except the endpoints of that edge).

(β) No supporting plane of a face translated by vector $\vec{\jmath}$ or $-\vec{\jmath}$ contains a vertex.

Let $\mathcal{I}$ denote the intersection, if not empty, of the supporting plane of a face with the translation by $\pm\vec{\jmath}$ of the supporting plane of another face. By assumption (β), $\mathcal{I}$ is a line.

(γ) No vertices project along the y-axis onto such a line $\mathcal{I}$.

(δ) For any point A on a face and with half-integer x and y-coordinates, $A \pm \vec{\jmath}$ does not belong to another face. More generally, no line $\mathcal{I}$ crosses any vertical line defined by half-integer x and y-coordinates.

This general position assumption is done with no loss of generality because it can be achieved by a sequence of four symbolic perturbations of decreasing importance: (i) the input faces are translated in the x-direction by ϵ_1, (ii) translated in the y-direction by ϵ_2, (iii) the vector $\vec{\jmath}$ is scaled by a factor $(1+\epsilon_3)$, and (iv) the faces are rotated by an angle ϵ_4 around a line that is not parallel to the coordinate axes. As shown below, enforcing $\epsilon_1 \gg \epsilon_2 \gg \epsilon_3 \gg \epsilon_4$ yields that our perturbation scheme removes all degeneracies.

Consider an intersection $\mathcal{I}$ as defined above; $\mathcal{I}$ can be a line or a plane. If $\mathcal{I}$ is a line L that induces a degeneracy of type (δ), this degeneracy is avoided by a translation (i) in the x-direction if L is not parallel to the xz-plane, and by a translation (ii) in the y-direction, otherwise. Then, perturbations (iii) and (iv) of smaller scales do not reintroduce this degeneracy [2]. If the intersection $\mathcal{I}$ is a plane, this remains the case after perturbations

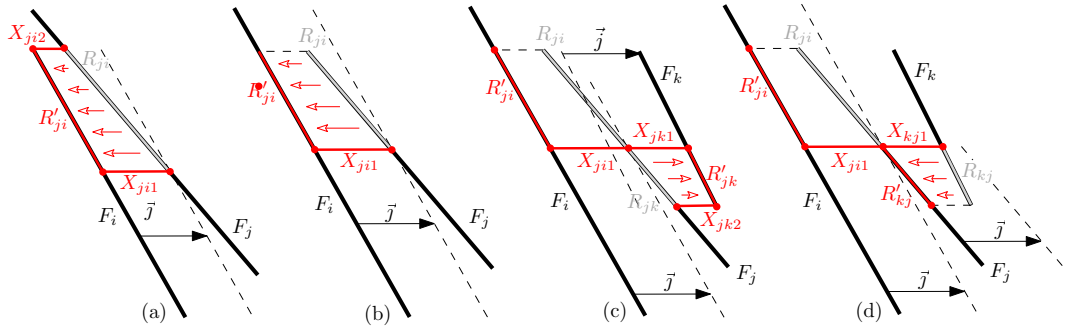

Figure 1 View inside a side wall $x = \text{cst}$. (a-d): The face F_j is partially projected onto F_i $(i < j)$, i.e., R_{ji} is replaced by the faces R'_{ji}, X_{ji1} and, in (a), X_{ji2}. (c): F_j is also partially projected onto F_k $(i < k < j)$. (d): If instead $i < j < k$, it is F_k that is partially projected onto F_j.

(i) and (ii), but the intersection becomes empty after a small enough perturbation (iii) and it remains empty after perturbation (iv). Hence, degeneracies of type (δ) are avoided by our scheme of perturbations.

Degeneracies of type (β) and (γ) are not affected by perturbations (i) and (ii), but they are avoided by the scaling of type (iii). Indeed, if $\mathcal{I}$ is a line then, viewed in projection on the back wall, the scaling of type (iii) translates the line. Finally, degeneracies of type (α) are not affected by perturbations (i-iii), but they are avoided by a rotation of type (iv).

2 Algorithm

We first describe the main algorithm in Section 2.1 and then two algorithmic refinements in Section 2.2 that we present separately for clarity. Our algorithm has the following property.

▶ **Theorem 1.** *Given a set $\mathcal{P}$ of polygonal faces in 3D in general position and that do not properly intersect, the algorithm outputs a simplicial complex $\mathcal{Q}$ whose vertices have integer coordinates and a mapping σ that maps every face F of $\mathcal{P}$ onto a set of faces (or edges or vertices) of $\mathcal{Q}$ such that there exists a continuous motion that moves every face F into $\sigma(F)$ such that (i) the L_∞ Hausdorff distance between F and its image during the motion never exceeds $\frac{3}{2}$ and (ii) if two points on two faces become equal during the motion, they remain equal through the rest of the motion.*

2.1 Main algorithm

The algorithm is organized in 4 steps. In every step of the algorithm, faces are subdivided and/or modified. We denote by $\mathcal{P}_i$ the set of faces at the end of Step i and by σ_i the mapping from the faces of $\mathcal{P}_{i-1}$ to those of $\mathcal{P}_i$ (with $\mathcal{P}_0 = \mathcal{P}$ and $\mathcal{P}_4 = \mathcal{Q}$). These mappings are trivial and not explicitly described, except in Step 1. Let $\sigma = \sigma_4 \circ \cdots \circ \sigma_1$ be the global mapping from the faces of $\mathcal{P}$ to those of the output simplicial complex $\mathcal{Q}$.

1. *Collapse the faces that are close to one another.* Order all the input faces arbitrarily from $\bar{F}_1$ to $\bar{F}_n$. During the process, we modify iteratively the faces. For clarity, we denote by F_i the faces that are iteratively modified, which we initially set to $F_i = \bar{F}_i$ for all i. Roughly speaking, for i from 1 to $n-1$, we project along y the points of $F_{i+1}, \ldots, F_n$ onto F_i but only the points that project at distance at most 1. Furthermore, we create, if

needed, side walls that connect the boundary of the projected points to their pre-image. Refer to Figure 1.

a. For i from 1 to n and for j from $i+1$ to n, do
- Let R_{ji} be the polygonal region that consists of the points $p_j \in F_j$ whose projection onto F_i along the y-direction lies within distance less than 1 from p_j, i.e., $R_{ji} = \{p_j \in F_j \mid \exists\, \alpha \in (-1,1),\, \exists p_i \in F_i,\, p_j = p_i + \alpha\vec{j}\}$.[1]
- Modify F_j by removing R_{ji} from it.

Let $\tilde{F}_1, \ldots, \tilde{F}_n$ be the resulting faces at the end of the two nested loops and let R'_{ji} be the projection of R_{ji} on $\tilde{F}_i$ along the y-direction.[2]

b. For j from 1 to n, consider on $\bar{F}_j$ the set of R_{ji} $(i < j)$ and consider their edges, in turn. We define new faces that connect some edges of R_{ji} and R'_{ji}, which we refer to as *connecting faces* (see e.g., faces $X_{ji\xi}$ in Figure 1). If edge e is a common edge of R_{ji} and $\tilde{F}_j$, we define a new face as the convex hull of e and its projection on F_i along y. If e is a common edge of R_{ji} and $R_{ji'}$ and if e projects (along y) on $\tilde{F}_i$ and on $\tilde{F}_{i'}$ into two distinct segments e_i and $e_{i'}$, respectively, we define a new face as the convex hull of e_i and $e_{i'}$; however, if e belongs to that face, we split it in two at e.[3]

c. For i from 1 to n, subdivide $\tilde{F}_i$ by the arrangement of edges of the R'_{ji}, $j = i+1, \ldots, n$.

To summarize, we have removed from every input face $\bar{F}_j$ the regions R_{ji}, $i = 1, \ldots, j-1$, we subdivided the resulting faces $\tilde{F}_i$ by the edges of all R'_{ji}, $j = i+1, \ldots, n$, and we created new connecting faces.

Finally, we define σ_1 to map every input face $\bar{F}_j$ to the union of the resulting face $\tilde{F}_j$, all the regions R'_{ji}, $i < j$ (subdivided as in $\tilde{F}_i$), and all the connecting faces that are defined by R_{ji}, $i < j$.

2. *Partition the space into slabs.* Project all the faces of $\mathcal{P}_1$ on the floor, compute their arrangement, lift all the resulting edges onto all faces of $\mathcal{P}_1$, and subdivide the faces accordingly; let $\mathcal{P}'_1$ be the resulting subdivision. Then, project all edges of $\mathcal{P}'_1$ on the back wall and compute their arrangement (but do not lift the resulting edges back on $\mathcal{P}'_1$).

The closed region bounded by the two side walls $x = c \pm \frac{1}{2}$, $c \in \mathbb{Z}$, is called a *thin slab* $\mathcal{S}_c$, if it contains (at least) a vertex of any of these two arrangements. A *thick slab* is a closed region bounded by two consecutive thin slabs.

We subdivide all faces of $\mathcal{P}'_1$ by intersecting them with the side-wall boundaries of all slabs, resulting in $\mathcal{P}_2$.

Note that if two thin slabs share a side-wall plane, this plane is a thick slab between these two thin slabs. However, we treat such thick slabs as if they had infinitesimal width; their two side-wall boundaries are considered combinatorially distinct although they coincide geometrically. Thus, for instance, an edge of $\mathcal{P}'_1$ intersects such a thick slab boundary in two combinatorially distinct points that geometrically coincide.

---

[1] R_{ji} is polygonal since its boundary consists of (i) segments of the boundary of F_j, (ii) segments of the boundary of F_i projected onto F_j along the y-direction, and (iii) segments of the intersection of F_j and the translated copies of F_i by vectors $\pm\vec{j}$.

[2] In the nested loops, for $i = i_0$, we modify F_j for $j > i_0$ by removing R_{ji_0} from F_j and, in particular, we do not modify any F_i for $i \leqslant i_0$. Hence, from the time when any R_{ji_0} is defined, we do not modify F_{i_0} and thus $F_{i_0} = \tilde{F}_{i_0}$.

[3] Connecting faces are trapezoids that intersect any side wall in segments of length at most 1 that are parallel to the y-axis. However, connecting faces may overlap and that a connecting face may not contain the edge of R_{ji} that defines it (see the full version for details).

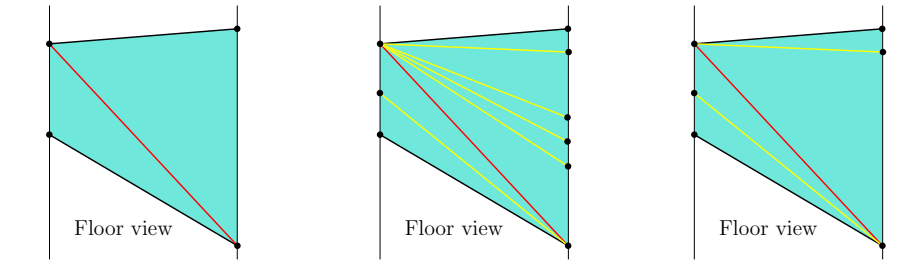

(a) Triangulation of trapezoids not considering dummy vertices.

(b) Same as (a) but with dummy vertices.

(c) Same as (b) but on a single trapezoid.

Figure 2 Triangulations of trapezoids in a thick slab.

3. *Triangulate the faces.* We triangulate all the faces of $\mathcal{P}_2$ in every slab in turn. We first consider thin slabs and then thick slabs. This order matters because, when triangulating faces in thin slabs, we split some edges at some new vertices; when such edges and new vertices lie in the side-wall boundaries of the thin slabs, they also belong to the adjacent thick slabs and these new vertices are to be considered in these thick slabs.

   a. *Thin slabs.* Project along the x-axis all the faces in a thin slab $\mathcal{S}_c$ on the side wall $x = c$ that bisects the slab, and compute the arrangement of the projected edges. In that side wall, denote as *hot* all the pixels that contain a vertex of that arrangement and split every edge that intersects a hot pixel at its intersection with the pixel boundary.[4] Triangulate the resulting arrangement[5] and lift it back (still along the x-axis) onto all the faces in the slab and subdivide them accordingly. The subdivision vertices that lie on the side-wall boundaries of $\mathcal{S}_c$ are referred to as *dummy vertices* to distinguish them from other vertices. In a thick slab of zero width, the dummy vertices typically differ on the two combinatorially-distinct though geometrically-equal side-wall boundaries.

   b. *Thick slabs.* Refer to Figure 2. Not considering the dummy vertices of Step 3a, all faces are trapezoids (possibly degenerated to triangles) such that the parallel edges lie on the two side-wall boundaries of the thick slab; any two trapezoids are either identical, disjoint, or share exactly one edge or vertex, and the same holds for their projections on the floor. The dummy vertices lie on the trapezoid edges that lie on the side-wall boundaries of the thick slab.

   Not considering the dummy vertices, all trapezoids that project on the floor onto one and the same trapezoid are triangulated such that all the diagonals project on the floor onto one and the same diagonal. Trapezoids can have dummy vertices only on the edges on the side walls; thus, after splitting a trapezoid in two triangles, each triangle can have dummy vertices on at most one of its edges. For every such triangle, we further triangulate it by adding an edge connecting every dummy vertex to the opposite vertex of the triangle.

[4] As in [7], these vertices are associated with the hot pixel so that the center of the pixel they will be snapped to is well defined. This ensures that no intersection is created during the snapping motion, but simply adding one vertex on the edges and strictly inside every hot pixel yields the same result.

[5] Before triangulating, add the hot pixel boundaries to the arrangement so that the triangulating edges do not cross hot pixels. Although triangulating the faces at this stage is useful for the proof of correctness of the algorithm, it improves the complexity without changing the output to triangulate these faces at the end of the algorithm instead; see Section 2.2.

4. *Snap all vertices* to the centers of their voxels. Vertices that are on the boundary of a thin slab $\mathcal{S}_c$ are snapped onto the side wall $x = c$ that bisects the slab; this is well defined even when two thin slabs share a side-wall boundary because we have considered (in Step 2) two combinatorial instances of such side walls, one associated to each of the thin slabs. Vertices that lie on the common boundary of two voxels inside a thin slab $\mathcal{S}_c$ are associated to voxels according to the vertex-pixel associations when snap rounding in 2D the projections of the edges in $\mathcal{S}_c$ onto its bisecting side wall $x = c$.

2.2 Algorithm refinements

Subdivision of the faces in thin slabs (Step 3a). When snapping all vertices to their voxel centers in Step 4, any planar polygon in a thin slab $\mathcal{S}_c$ is transformed into a planar polygon in the side-wall $x = c$. Depending on how the vertices move toward their voxel centers, the polygon may not remain planar during the motion, but it is planar at the end of the motion. Hence, the output will be unchanged if, in Step 3a, we avoid triangulating the faces, that is, we avoid triangulating the arrangement in the side wall $x = c$ and only lift the new vertices of the arrangement onto the edges in $\mathcal{S}_c$. Still, after snapping the vertices in Step 4, the resulting polygons in the side wall $x = c$ should be triangulated so that the algorithm returns a simplicial complex.

Subdivision of the connecting faces (Steps 2, 3a and 3b). In Step 2, the connecting faces are subdivided by the side-wall boundaries of all slabs. The resulting faces are trapezoids (possibly degenerate to triangles) with two edges of length at most 1 that are parallel to the y-axis. Such trapezoids remain planar when their vertices are moved to their voxel centers in Step 4. Hence, triangulating these trapezoids does not modify the motion of any of its points. Furthermore, subdividing their edges that are parallel to the y-axis does not change the trapezoid motions either.

It follows that, in Step 2, we do not need to subdivide the connecting faces by the vertical projections of the edges of $\mathcal{P}_1$, in Step 3a, we do not need to lift any dummy vertices on the connecting-face edges that are parallel to the y-axis and in Step 3b, we do not need to triangulate the connecting faces. Still, we should triangulate the connecting faces at the end of the algorithm in order to obtain a simplicial complex which could trivially be done.

3 Proof of correctness

We prove here Theorem 1. We focus on Step 1 of the algorithm in Section 3.1, on Step 4 in Section 3.2, and we wrap up in Section 3.3.

3.1 Step 1

We first prove the main properties of Step 1 and then a technical lemma, which will be used in Lemma 6.

▶ **Lemma 2.** *Every point of the faces of $\mathcal{P}$ can be continuously moved so that every face F of $\mathcal{P}$ is continuously deformed into $\sigma_1(F)$ such that (i) the L_∞ Hausdorff distance between F and its image during the motion never exceeds 1 and (ii) if two points on two faces become equal during the motion, they remain equal through the rest of the motion.*

Sketch of proof. The complete proof is omitted for lack of space. The motion is decomposed into n successive phases, considering the projection on each F_i in turn. For a particular F_i, the naive way of moving R_{ji} to $\sigma_1(R_{ji})$ is to move R_{ji} to R'_{ji}, by moving each point of

R_{ji} along the y-direction and at constant speed, and to transform edge e_ζ into face X_ζ for every edge e_ζ of the boundary of R_{ji} that defines a connecting face X_ζ. However, this does not define a function since segments are mapped to faces. The definition of a continuous motion requires a bit of technicality but the straightforward underlying idea is to subdivide R_{ji} by considering, for each edge e_ζ, a tiny quadrilateral inside R_{ji} and bounded by e_ζ. We then transform continuously each tiny quadrilateral bounded by e_ζ into the connecting face X_ζ and move the complement of these quadrilaterals, which is a slightly shrunk version of R_{ji}, into R'_{ji}. This can be done so that when two distinct points become equal during the motion, they remain equal through the rest of the motion. The Hausdorff distance property is straightforward. ◀

▶ **Lemma 3.** *If a line L parallel to the y-axis intersects the relative interior of a face of $\mathcal{P}_1$ in a single point p then the distance along L from p to any other face of $\mathcal{P}_1$ is at least 1.*

Proof. If a line L parallel to the y-axis intersects the relative interior of a face F of $\mathcal{P}_1$ in a single point p, this face is not a connecting face. Assume for a contradiction that L intersects another face F' of $\mathcal{P}_1$ at some point p' that is at distance less than 1 from p.

Consider first the case where F' is not a connecting face. Since non-connecting faces are not parallel to the y-axis, there exists a line L' parallel to the y-axis (and close to L) that intersects the relative interiors of both F and F' in two points at distance less than 1. However, this is impossible after Step 1.

Consider now the case where F' is a connecting face. It follows from Step 1b of the algorithm that any point $p' \in F'$ lies on a segment (not necessarily entirely in F') of length at most 2, parallel to the y-axis and with its endpoints on two non-connecting faces of $\mathcal{P}_1$. Consider the shortest such segment. Unless this segment has length 2 and p is its midpoint, p is at distance less than 1 from one of the segment endpoints; considering instead of F' the non-connecting face supporting this endpoint yields a contradiction as shown above. By definition, if the segment has length 2, its midpoint p must lie on a common edge e of some R_{ji} and $R_{ji'}$ such that p projects on $\tilde{F}_i$ and on $\tilde{F}_{i'}$ into two points at distance 1 from p in the directions $\vec{\jmath}$ and $-\vec{\jmath}$, respectively. During Step 1, R_{ji} and $R_{ji'}$ are removed from the input face $\bar{F}_j$, thus the resulting face $\tilde{F}_j$ does not contain p in its interior (and not at all if p is in the interior of edge e). If the input face that contains F' is distinct from $\bar{F}_j$, then the fact that p belongs to $R_{ji} \cap R_{ji'} \subset \bar{F}_j$ and to the interior of F' contradicts the hypothesis that the input faces do not properly intersect. Otherwise, $F' \subseteq \bar{F}_j$ and thus $F' \subseteq \tilde{F}_j$, which contradicts the fact that p belongs to the interior of F' but not to the interior of $\tilde{F}_j$, and concludes the proof. ◀

3.2 Step 4

In the following, we consider in the snapping phase of Step 4 a continuous motion of the vertices such that every vertex moves on a straight line toward the center of its voxel at a speed that is constant for each vertex and so that all vertices start and end their motions simultaneously. The motion of the other points in a face move accordingly to their barycentric coordinates in the face. Note that, in every voxel that contains a vertex, the motion is a homothetic transformation whose factor goes from one to zero. During that motion, we consider that thin and thick slabs respectively shrink and expand accordingly.

We recall the standard snap-rounding result for segments in two dimensions. A pixel is called *hot* if it contains a vertex of the arrangement of segments.

▶ **Theorem 4** ([7, Thm. 1]). *Consider a set of segments in 2D split in fragments at the hot pixel boundaries and a deformation that (i) contracts homothetically all hot pixels at the same speed*[6] *and (ii) moves the fragments outside the hot pixels according to the motions of their endpoints. During the deformation, no fragment endpoint ever crosses over another fragment.*

▶ **Lemma 5.** *When moving all vertices to the center of their voxels in Step 4, no two faces, edges, or vertices of $\mathcal{P}_3$ properly intersect in thin slabs.*

Proof. Consider all the faces of $\mathcal{P}_3$ in a thin slab $\mathcal{S}_c$ and the arrangement of their projections (along the x-axis) onto the side wall $x = c$. In that side wall, a pixel that contains a vertex of the arrangement is hot and every edge (in that side wall) that intersects a hot pixel is split at the pixel boundary (Step 3a). By Theorem 4, when moving in that side-wall all the projected vertices to the centers of their pixels, the topology of the arrangement does not change except possibly at the end of the motion, where edges and vertices may become identical.

It follows that the property that every face of $\mathcal{P}_3$ in $\mathcal{S}_c$ projects onto a single face of the arrangement in the side wall $x = c$, which holds by construction at the beginning of the motion (Step 3a), holds during the whole motion of the vertices in 3D and of their projections in the side wall $x = c$.

Furthermore, the motion preserves the ordering of the x-coordinates of the vertices in $\mathcal{S}_c$, until the end when they all become equal to c. Together with the previous property, this implies that, in a thin slab, during the snapping motion, (i) no vertices and edges intersect the relative interior of a face and (ii) if two edges intersect in their relative interior, it is at the end of the motion and they become identical. Furthermore, (iii) no vertices intersect the relative interior of an edge because, in Step 3a, we have split every edge that intersects a hot pixel in projection in the side wall $x = c$. This concludes the proof. ◀

▶ **Lemma 6.** *When moving all vertices to the center of their voxels in Step 4, no two faces, edges, or vertices of $\mathcal{P}_3$ properly intersect in thick slabs.*

Proof. By construction (Step 2), all the vertices in a thick slab are on its side-wall boundaries and, in these side walls, no two edges or vertices properly intersect during the motion, by Lemma 5. Thus, we only have to consider edges that connect the two side-wall boundaries of a thick slab and show that such edges do not properly intersect during the snapping motion. Note that input faces are not vertical (i.e., not parallel to the z-axis) by assumption and connecting faces are not vertical in thick slabs since they are parallel to the y-axis and they intersect both side-wall boundaries of the thick slab.

Initially, these edges project on the floor onto edges that do not properly intersect pairwise (by definition of the slabs in Step 2). Thus, by Theorem 4, the projections on the floor of two edges either (i) coincide throughout the whole motion, or (ii) they do not properly intersect and do not coincide throughout the whole motion except possibly at the end when they may coincide. In the first case, throughout the whole motion, the edges belong to the same moving vertical plane and they do not properly intersect since they do not initially; indeed, since faces are not vertical, edges may intersect in a vertical plane only if they are boundary edges of trapezoids of $\mathcal{P}_2$, and such edges do not properly intersect on the back wall by definition of thick slabs. Hence, only in the latter case (ii), two edges may properly

[6] The proof in [7] considers separately motions in x and in y but the same argument applies for simultaneous homothetic contractions in x and y.

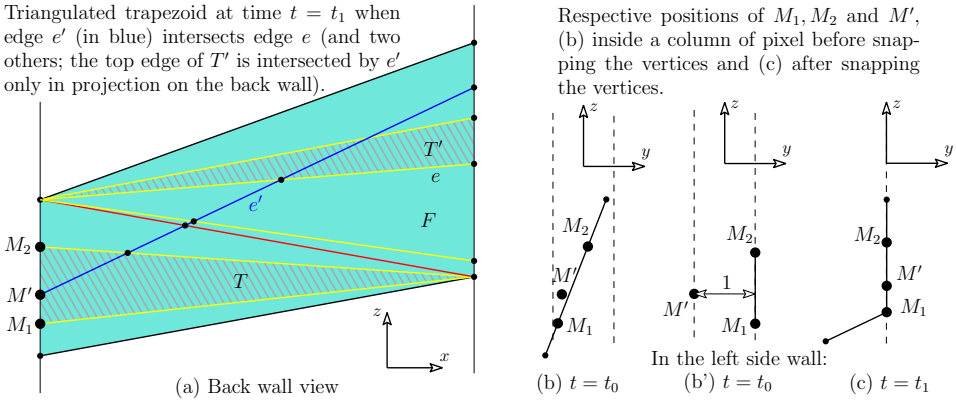

Figure 3 For the proof of Lemma 6.

intersect during the motion; furthermore, the first time this may happen is at the end of the motion and then, the two edges belong to the same vertical plane.

Similarly, applying Theorem 4 to the back-wall projection of the boundary edges of the trapezoids (but not of their triangulating edges), we get that if two boundary edges of trapezoids properly intersect in 3D during the motion, it is at the end and they must coincide in the back-wall projection. Since two edges that coincide in two projections are equal, we get that boundary edges of trapezoids cannot properly intersect throughout the motion. It remains to prove that there is no proper intersections that involve the edges triangulating the trapezoids.

Consider for a contradiction two edges e and e' that properly intersect in a vertical plane V at time t_1, the end of the motion. Since boundary edges of the trapezoids do not properly intersect, one of the two edges, say e, is a triangulation edge. Consider the trapezoid that initially contains e and its image F, at time t_1, which is a set of triangles. We prove that (at time t_1) **edge e' properly intersects (at least) one of the two boundary edges of F.**

Assume for a contradiction that e' properly intersects none of the two boundary edges of F and refer to Figure 3(a). Consider all the edges of the triangulation of F that are properly intersected by e' and the sequence of triangles (of that triangulation) that are incident to these edges; let T and T' denote the first and last triangles of that sequence. All these triangles except possibly one, T or T', must be in the vertical plane V; this is trivial for all triangles but T and T' and, if neither T nor T' lies in V, then edge e' properly intersects the surface formed by these triangles, contradicting the property that t_1 is the first time a proper intersection may occur.

As in Figure 3(a), assume without loss of generality that T, the bottommost triangle of the sequence, lies in the vertical plane V at time t_1. Let M' be the endpoint of e' that lies in T and let M_1M_2 be the edge of T that supports M'. At time t_1, M_1 and M_2 are vertically aligned and M' is in between them. Thus, before the snapping motion starts, at time $t = t_0$, M_1, M_2 and M' must lie in the same vertical column of pixel (in the side wall) and M' must be vertically in between M_1 and M_2 (see Figure 3(b)). However, the distance along the y-axis between M' and segment M_1M_2 is at least 1 by Lemma 3. Thus, M' and $M' \pm \vec{\jmath} \in M_1M_2$ are initially on opposite sides of the column of pixels (as in Figure 3(b')) and thus have half-integer x and y-coordinates, which contradicts item (δ) of our general position hypothesis.

Hence, at time $t = t_1$, edge e' properly intersects one of the boundary edges, say r, of trapezoid F. Since boundary edges do not properly intersect, e' must be a triangulation edge of its trapezoid F' and we can apply the same argument as above on edges e' and r, instead of e and e'. We get that r properly intersects a boundary edge r' of F', which is a contradiction. ◀

3.3 Wrap up, proof of Theorem 1

First, by construction, the algorithm outputs faces that have integer coordinates.

Second, there is a continuous motion of every input face F into $\sigma(F)$ so that the Hausdorff distance between F and its image during the motion never exceeds $\frac{3}{2}$ for the L_∞ metric. Indeed, by Lemma 2, the Hausdorff distance never exceeds 1 between F and its image during the motion Step 1; in Steps 2 and 3 the faces are only subdivided; and the Hausdorff distance between any face of $\mathcal{P}_3$ and and its image during the motion of Step 4 clearly never exceeds $\frac{1}{2}$.

Third, if two points on two faces become equal during the motion, they remain equal through the rest of the motion. This is proved in Lemma 2 for the motion of Step 1 and this also holds for the motion of Step 4 since, by Lemmas 5 and 6, if two faces, edges or vertices intersect during this motion, they share a common face of both, whose motion is uniquely defined by its vertices (actually, we show in the proofs of Lemmas 5 and 6 that no two distinct points become equal except possibly at the end of the motion).

Finally, the algorithm outputs a simplicial complex by Lemmas 5 and 6.

4 Worst-case complexity

We define the z-cylinder of a face F as the volume defined by all the lines parallel to the z-axis that intersect F; similarly for x and y-cylinders. Over all input faces F, let f_d be the maximum number of input faces that are (i) intersected by one such cylinder of F and (ii) at distance at most d from F. Denote by $f = f_\infty$ the maximum number of faces intersected by one such cylinder. Let w_x be the maximum number of input faces that are intersected by any side wall $x = c$.

▶ **Proposition 7.** *Given a set of $O(n)$ polygons, each of constant complexity, the algorithm outputs a simplicial complex of complexity $O(nw_x^2 f^7 f_1^5)$ in time $O(n^2 w_x f^9 f_1^7)$.*

Proof. For analyzing the complexities of the algorithm and of its output, we bound the number of edges that we consider for splitting the input faces. However, for each face, we first count the number of edges without considering any intersection; in other words, for each face, we bound the number of lines supporting the edges instead of the complexity of the induced arrangement. To avoid confusion, we refer to these edges as unsplit edges.

Number of slabs. After projection on the back wall, the edges of R_{ji} and R'_{ji}, in Step 1, are pieces of the boundary edges of the input faces $\bar{F}_k$ and of the segments of intersection $\bar{F}_k \cap (\bar{F}_\ell \pm \vec{\jmath})$. In a y-cylinder of a face F, only f faces project on the back wall and thus there are $O(ff_1)$ such edges. Thus, at the end of Step 1, every input face ends up supporting $O(ff_1)$ unsplit edges. In Step 2, we thus lift $O(f^2 f_1)$ unsplit edges onto every face. Every unsplit edge on a given face F may only intersect, after projection on the back wall, edges that lie on the faces that intersect the y-cylinder of F; there are $O(f)$ such faces and $O(f^2 f_1)$ unsplit edges on each of them, thus every unsplit edge may intersect $O(f^3 f_1)$ edges on the back wall. There are $O(nf^2 f_1)$ unsplit edges in total, hence, in Step 2, the back wall arrangement has complexity $O(nf^5 f_1^2)$. (Similarly, the floor arrangement has complexity $O(nf^3 f_1^2)$.) The number of thin and thick slabs is thus $O(nf^5 f_1^2)$.

Complexity in thin slabs. For any thin slab $\mathcal{S}_c$, we analyze the complexity of the output in the side wall $x = c$. We do not consider here any triangulation edge inside the faces as discussed in Section 2.2. Thus, the edges in $\mathcal{S}_c$ are subdivisions of the edges of $\mathcal{P}_1$ and subdivisions of the edges defined as the intersection of the faces of $\mathcal{P}_1$ and the side walls $x = c \pm \frac{1}{2}$. More precisely, these edges are pieces of either (a.i) edges of $\mathcal{P}_1$ that lie on the input faces, (a.ii) edges of intersection of an input face with a side wall $x = c \pm \frac{1}{2}$, (b.i) edges of connecting faces that are parallel to the y-axis, or (b.ii) edges of intersection of a connecting face with a side wall $x = c \pm \frac{1}{2}$. Note that, although we do not consider the faces triangulated in $\mathcal{S}_c$, the edges are subdivided according to the arrangement of their projections on the side wall $x = c$; however, we consider them unsplit for now.

As mentioned above, every input face supports $O(ff_1)$ unsplit edges at the end of Step 1. Thus, if $F_{\mathcal{S}_c}$ denotes the number of input faces that are intersected by the thin slab $\mathcal{S}_c$, there are $O(F_{\mathcal{S}_c} ff_1)$ edges of types (a) in $\mathcal{S}_c$. On the other hand, the $O(ff_1)$ unsplit edges on the back wall yield an arrangement of size $O(f^2 f_1^2)$; viewed on the back wall, edges of type (b) are incident to the vertices of this arrangement, so the number of edges of type (b) in $\mathcal{S}_c$ is bounded by $O(F_{\mathcal{S}_c} f^2 f_1^2)$.

We bound the number of intersections between these edges at the end of the algorithm. However, as noted in Section 2.2, we do not consider intersections that involve edges of type (b) because such intersections necessarily belong to the hot pixels defined by the edge endpoints. We thus consider here only edges of type (a). Every edge on a given input face F may only intersect, after projection on the side wall $x = c$, edges that lie on faces that intersect $\mathcal{S}_c$ and the x-cylinder of F; there are $O(f_1)$ such faces and $O(ff_1)$ edges on each of them, thus every edge may intersect $O(ff_1^2)$ edges on the side wall $x = c$. There are $O(F_{\mathcal{S}_c} ff_1)$ edges of type (a) in $\mathcal{S}_c$, thus, there are $O(F_{\mathcal{S}_c} f^2 f_1^3)$ intersections between edges of type (a).

In addition to these $O(F_{\mathcal{S}_c} f^2 f_1^3)$ intersections, there are $O(F_{\mathcal{S}_c} f^2 f_1^2)$ edges (and thus edge endpoints) in $\mathcal{S}_c$. The number of hot pixels in the side wall $x = c$ is thus $H_c = O(F_{\mathcal{S}_c} f^2 f_1^3)$ at the end of Step 3a.

The number of vertices (dummy or not) in $\mathcal{S}_c$ at the end of Step 3a is the number of hot pixels, H_c, times the number of edges in $\mathcal{S}_c$, $O(F_{\mathcal{S}_c} f^2 f_1^2)$. However, the size of the arrangement in the side wall $x = c$ after snapping the vertices to their voxel centers in Step 4 is of the order of the number of hot pixels, H_c, and it remains as such after triangulating the faces (see Section 2.2).

Complexity in thick slabs. The number of edges in a thick slab after the triangulation of Step 3b is (i) the number of edges of connecting faces in the slab, that is $O(w_x ff_1)$ (the number $O(ff_1)$ of unsplit edges on input faces times the number $O(w_x)$ of input faces that intersect the slab) plus (ii) the number $O(w_x)$ of input faces that intersect the slab times the number $H_{c_1} + H_{c_2}$ of hot pixels in the adjacent thin slabs $\mathcal{S}_{c_1}$ and $\mathcal{S}_{c_2}$. This sums up to $O(w_x(H_{c_1} + H_{c_2}))$.

Complexity of the output. The total complexity of the output is thus $O(w_x)$ times the sum over all thin slabs of the number of hot pixels H_c in $\mathcal{S}_c$. Denoting by $\mathring{F}_{\mathcal{S}_c}$ the number of input faces that are entirely inside $\mathcal{S}_c$, we have that $F_{\mathcal{S}_c} \leqslant \mathring{F}_{\mathcal{S}_c} + 2w_x$ and that the sum over all thin slabs of $\mathring{F}_{\mathcal{S}_c}$ is $O(n)$. Hence, the sum over all $N = O(nf^5 f_1^2)$ thin slabs of the numbers of hot pixels $H_c = O(F_{\mathcal{S}_c} f^2 f_1^3)$ is $O((n + Nw_x) f^2 f_1^3) = O(nw_x f^7 f_1^5)$. Times w_x gives the complexity of the output: $O(nw_x^2 f^7 f_1^5)$.

Time complexity. The time complexity is straightforward given the above analysis and the observation that the complexity of $\mathcal{P}_3$ can be larger than the rounded output. ◀

5 Complexity under some assumptions

We consider, in the following proposition, the complexity of our algorithm for approximations of "nice" surfaces, defined as follows.

▶ **Definition 8.** An (ε, κ)-sampling of a surface $\mathcal{S}$ is a set of vertices on $\mathcal{S}$ so that there is at least 1 and at most κ vertices strictly inside any ball of radius ε centered on $\mathcal{S}$. It is straightforward that a (ε, κ)-sampling of a fixed compact surface has $\Theta(n)$ vertices with $n = \frac{1}{\varepsilon^2}$ (the constant hidden in the Θ complexity depends on the area of the surface).

▶ **Definition 9.** The Delaunay triangulation of a set of points $\mathcal{P}$ restricted to a surface $\mathcal{S}$ is the set of simplices of the Delaunay triangulation of $\mathcal{P}$ whose dual Voronoi faces intersect $\mathcal{S}$. If $\mathcal{P} \subset \mathcal{S}$, we simply refer to the restricted Delaunay triangulation of $\mathcal{P}$ on $\mathcal{S}$.

▶ **Definition 10** (Nice surfaces)**.** A surface $\mathcal{S}$ is k-monotone (with respect to z) if every line parallel to the z-axis intersects $\mathcal{S}$ in at most k points. Let Δ and k be any two positive constants. A surface $\mathcal{S}$ is *nice* if it is a compact smooth k-monotone surface such that the Gaussian curvature of $\mathcal{S}$ is larger than a positive constant in a ball of radius Δ centered at any point $p \in \mathcal{S}$ where the tangent plane to $\mathcal{S}$ is vertical.

For instance, a compact smooth algebraic surface whose silhouette (with respect to the vertical direction) is a single convex curve is nice for suitable choices of Δ and k.

▶ **Remark 11.** *The following complexities are asymptotic when n goes to infinity (or ε to zero) with hidden constants depending on the surface areas, Δ, and k. It is important to notice that these complexities are independent from the voxel size, which can go to zero with no changes in the complexities. Of course if the grid size and the surface are fixed, the total number of voxels intersecting the surface is constant and so is the size of a rounding.*

The following lemma is a technical though rather straightforward result, whose proof is omitted for lack of space.

▶ **Lemma 12.** *The restricted Delaunay triangulation $\mathcal{T}$ of a (ε, κ)-sampling of a nice surface has complexity $O(n) = O(\frac{1}{\varepsilon^2})$. Any plane $x = c$ intersects at most $O(\sqrt{n}) = O(\frac{1}{\varepsilon})$ faces of $\mathcal{T}$. Furthermore, for any face f of $\mathcal{T}$, the set of vertical lines through f intersects at most $O(n^{\frac{1}{4}}) = O(\frac{1}{\sqrt{\varepsilon}})$ faces of $\mathcal{T}$.*

▶ **Proposition 13.** *Given the arrangement of the restricted Delaunay triangulations of the (ε, κ)-samplings of a constant number of nice surfaces, the algorithm outputs a simplicial complex of complexity $O(n^5)$ in time $O(n^6\sqrt{n})$.*

Proof. Consider the restricted Delaunay triangulations of the (ε, κ)-samplings of two surfaces. By definition of (ε, κ)-samplings, it is straightforward that any triangle of one triangulation intersects a constant number of triangles of the other triangulation. Hence, the complexities of Lemma 12 hold for the arrangement of the two triangulations, and similarly for a constant number of triangulations. Thus, for the arrangement of triangulations, Lemma 12 yields $w_x = O(\sqrt{n})$ and $f_1 < f = O(\sqrt[4]{n})$ (as defined in Section 4) and plugging these values in the complexities of Proposition 7 yields the result. ◀

▶ **Remark 14.** *In practice on realistic data, one can anticipate better time and space complexities of $O(n\sqrt{n})$. Indeed, $f_1 < f$ should behave as if they were in $O(1)$ and in 2D arrangements, hot pixels are usually intersected by $O(1)$ segments. Then, with $w_x = O(\sqrt{n})$ as in Lemma 12, the proof of Proposition 7 yields complexities in $O(n\sqrt{n})$.*

Acknowledgements

The authors would like to thank André Lieutier for having initially pointed out the problem and its significance for industry, and for many discussions on the problems, Hazel Everett, Mark de Berg, Danny Halperin, Raimund Seidel, and Dave Bremner.

References

1 Mark de Berg, Dan Halperin, and Mark Overmars. An intersection-sensitive algorithm for snap rounding. *Computational Geometry*, 36(3):159–165, 2007. doi:10.1016/j.comgeo.2006.03.002.

2 Olivier Devillers, Menelaos Karavelas, and Monique Teillaud. Qualitative Symbolic Perturbation: Two Applications of a New Geometry-based Perturbation Framework. *Journal of Computational Geometry*, 8(1):282–315, 2017. doi:10.20382/jocg.v8i1a11.

3 Steven Fortune. Polyhedral modelling with multiprecision integer arithmetic. *Computer-Aided Design*, 29(2):123 – 133, 1997. Solid Modelling. doi:doi.org/10.1016/S0010-4485(96)00041-3.

4 Steven Fortune. Vertex-rounding a three-dimensional polyhedral subdivision. *Discrete & Computational Geometry*, 22(4):593–618, 1999. doi:10.1007/PL00009480.

5 Michael T. Goodrich, Leonidas J. Guibas, John Hershberger, and Paul J. Tanenbaum. Snap rounding line segments efficiently in two and three dimensions. In *Proceedings of the thirteenth annual symposium on Computational geometry*, pages 284–293. ACM, 1997. doi:10.1145/262839.262985.

6 Daniel H. Greene and F. Frances Yao. Finite-resolution computational geometry. In *Foundations of Computer Science, 1986., 27th Annual Symposium on*, pages 143–152. IEEE, 1986. doi:10.1109/SFCS.1986.19.

7 Leonidas J. Guibas and David H. Marimont. Rounding arrangements dynamically. *International Journal of Computational Geometry & Applications*, 8(02):157–178, 1998. doi:10.1142/S0218195998000096.

8 Dan Halperin and Eli Packer. Iterated snap rounding. *Computational Geometry*, 23(2):209–225, 2002. doi:10.1016/S0925-7721(01)00064-5.

9 John Hershberger. Improved output-sensitive snap rounding. *Discrete & Computational Geometry*, 39(1):298–318, Mar 2008. doi:10.1007/s00454-007-9015-0.

10 John Hershberger. Stable snap rounding. *Computational Geometry*, 46(4):403–416, 2013. doi:10.1016/j.comgeo.2012.02.011.

11 John D. Hobby. Practical segment intersection with finite precision output. *Computational Geometry*, 13(4):199–214, 1999. doi:10.1016/S0925-7721(99)00021-8.

12 V. Milenkovic and L. R. Nackman. Finding compact coordinate representations for polygons and polyhedra. *IBM Journal of Research and Development*, 34(35):753–769, 1990.

13 Victor Milenkovic. Rounding face lattices in d dimensions. In *Proceedings of the 2nd Canadian Conference on Computational geometry*, pages 40–45, 1990.

14 Eli Packer. Iterated snap rounding with bounded drift. *Computational Geometry*, 40(3):231 – 251, 2008. doi:doi.org/10.1016/j.comgeo.2007.09.002.